

I. APITZ
A. VOGEL 

Material ejection in nanosecond Er:YAG laser ablation of water, liver, and skin

Institut für Biomedizinische Optik, Universität zu Lübeck, Peter-Monnik-Weg 4, 23562 Lübeck, Germany

Received: 30 June 2004/Accepted: 20 December 2004
Published online: 2 March 2005 • © Springer-Verlag 2005

ABSTRACT We investigated the mechanisms of material ejection in Q-switched Er:YAG laser tissue ablation (70-ns pulse duration) where moderate and large radiant exposures are associated with large volumetric energy densities in the target material. For water, an initial phase of non-equilibrium surface vaporization is followed by an explosive vaporization of the superficial liquid volume from a supercritical state. The ablation of deeper layers with lower peak temperatures proceeds as phase explosion. For mechanically strong tissues, non-equilibrium surface vaporization is followed by a vapour explosion coupled with thermal dissociation of the biomolecules into volatile products. In deeper layers, ablation proceeds as confined boiling with mechanical tearing of the tissue matrix by the vapour pressure. The recoil stress induced at a radiant exposure of 5.4 J/cm^2 is in the order of 500–900 MPa. For water and soft tissues such as liver, the recoil causes a powerful secondary material expulsion. For stronger tissues such as skin, no secondary expulsion was observed even though the recoil stress largely exceeds the static tensile strength of the tissue. Recoil-induced material expulsion results in an increase of both ablation efficiency and mechanical side effects of ablation. Theoretical modelling of the succession of phase transitions in nanosecond-laser tissue ablation and of recoil-induced material expulsion remain a major challenge for future work.

PACS 42.62.Be; 79.20.Ds


1 Introduction

We showed recently that a phase explosion within the target material is the primary mechanism for material ejection when free-running Er:YAG laser pulses are used for ablation of water and soft tissues such as liver. For mechanically stronger tissues such as skin, the tensile strength of the tissue matrix is higher than the stresses resulting from the phase explosion, and ablation occurs only after a further pressure build-up through confined boiling [1, 2]. For liquids and mechanically weak tissues, the recoil induced by the primary material ejection causes a secondary material expulsion that largely increases the ablation efficiency [3].

When Q-switched Er:YAG laser pulses of 50–100 ns duration are employed, the rate of energy deposition into the tissue is more than 1000 times larger than with free-running laser pulses of durations in the range of several hundred microseconds. Since many authors have observed that ablation by nanosecond laser irradiation occurs largely toward the end and after the laser pulse [1], there is evidence that the rate of energy dissipation in the ablation process is considerably slower than the rate of energy deposition. Thus, much higher volumetric energy densities are produced in the target material than with free-running laser pulses, and the ablation process will be associated with other and more vigorous types of phase transitions and with a faster dynamics. For example, irradiation of water at a radiant exposure of 5 J/cm^2 will result in a volumetric energy density of 13 kJ/cm^3 at the water surface if ablation starts at the end of the laser pulse. Assuming a constant value of the heat capacity, this corresponds to a temperature rise of 3100 K (For a more precise estimate, one must consider the temperature dependence of the heat capacity.) At these temperatures the constituent molecules of the tissue matrix can be thermally dissociated into volatile fragments, and the volumetric energy density of 13 kJ/cm^3 is 10-fold larger than the energy density of 1.27 kJ/cm^3 required to initiate a phase explosion under atmospheric conditions [1]. It is the aim of the present study to elucidate how the extreme conditions produced during Q-switched Er:YAG laser tissue ablation modify the primary and recoil-induced material ejection. Because primary material ejection and recoil-induced material expulsion are largely determined by the mechanical strength of the extracellular tissue matrix (ECM) [1], we chose three target materials with different mechanical properties: skin (mechanically strong), liver (mechanically weak), and water (no matrix at all, but the main absorber for IR laser irradiation).

2 Experimental methods

We used a self-built Er:YAG laser that was Q-switched by a rotating mirror and delivered pulses with 70-ns duration and up to 11-mJ energy. We investigated the ablation process at radiant exposures between 0.123 J/cm^2 and 5.4 J/cm^2 , with spot sizes of 1 mm and 0.5 mm, respectively. The optical penetration depth of the Er:YAG laser irradiation in water is $1.3 \mu\text{m}$ at 1.02 J/cm^2 , and $4.6 \mu\text{m}$ at

 Fax: +49-451-505-486, E-mail: vogel@bmo.uni-luebeck.de

5.4-J/cm² radiant exposure (Fig. 6 in [1]). For this optical penetration depth and at a pulse duration of 70 ns, ablation is thermally confined but not stress confined [1].

Tissue experiments were performed *in vitro* on porcine liver and skin of pig's ears from a local slaughterhouse. The dynamics of water, liver, and skin ablation was recorded by bright-field photography and dark-field Schlieren photography at different time delays after the beginning of the laser pulse. The dark-field Schlieren technique [4] possesses a high sensitivity for 'phase objects' such as gaseous ablation products and acoustic transients that exhibit little optical absorption but deflect the light due to intrinsic refractive-index variations. Bright-field photography is well suited to image light-absorbing particles, but only strong pressure transients and parts of the gaseous plume exhibiting strong refractive-index gradients are visualized because they deflect part of the illuminating light out of the imaging aperture. We employed a frequency-doubled Nd:YAG laser coupled into a 300-m-long multimode optical fiber as light source for speckle-free Schlieren photography [5], and a flash discharge with 12-ns duration (Nanolite, High-Speed Photosystems, Wedel, Germany) for bright-field photography. Imaging optics with large F -number ($F = 9$ to $F = 15$) were used to enhance the visualization of phase modulations in bright-field photography. Larger F -numbers were avoided in order to maintain a reasonable diffraction-limited resolution. Images were recorded using a digital camera (Fujifilm S1 Pro) with 6 million pixels.

3 Primary material ejection

3.1 Phase transitions

The dynamics of water ablation at radiant exposures Φ of 0.12 J/cm², 1.4 J/cm², and 5.4 J/cm² is presented in Figs. 1 and 2. The dynamics is characterized by a succession of explosive vaporization, shock-wave emission, and ejection of very fine droplets. These droplets cannot be resolved on the photographs and appear as reddish haze. The reddish colour indicates that the droplet size is sufficiently small to cause Rayleigh scattering by which blue light is scattered much more strongly than red light [6]. As a consequence, mainly the red spectral components of the illumination light pass the imaging optics. The droplets are produced by a phase explosion of superheated liquid that spontaneously decomposes into a mixture of saturated vapour and saturated liquid [1, 2, 7]. For $\Phi = 0.12$ J/cm², almost the entire plume consists of fine droplets. The partitioning into vapour and liquid depends on the value of the volumetric energy density ε of the superheated liquid. For $\varepsilon > 2.59$ kJ/cm³ the energy density is larger than the vaporization enthalpy of water at room temperature under atmospheric pressure, and thus the entire liquid is explosively transformed into vapour. Such a 'vapour explosion' apparently characterizes the initial stages of the ablation process for radiant exposures of 1.4 J/cm² and 5.4 J/cm², where the top part of the ablation plume is completely transparent. After the end of the laser pulse, the ablation front continues to propagate in depth, and the volumetric energy density in the surface layers of the water sample decreases. When the energy density becomes smaller than the vaporization enthalpy of water, the super-

heated tissue water starts to decompose into vapour and liquid in a phase explosion, and droplet ejection commences [2]. Droplet ejection begins after ≈ 300 ns and lasts for a few microseconds. These observations are consistent with results of molecular dynamics simulations performed for ablation under thermal confinement at $1.75\times$ ablation threshold. The simulations predict that material ejected from the top layers of a molecular substrate decomposes into gas-phase molecules and a small fraction of very small clusters, while the middle and rear parts of the plume are composed of ever larger clusters [8].

When liver is ablated at a radiant exposure of 1.4 J/cm² (Fig. 3), the entire ablation plume consists of tissue fragments. However, at a radiant exposure of 5.4 J/cm² (Fig. 4), the top part of the plume is transparent, and only after about 200 ns are particulate fragments ejected. The succession of gaseous and particulate ablation products could be visualized only by a careful design of the photographic setup. It was previously mistaken by some researchers as a start of the ablation process well after the end of the laser pulse, because they observed only the particulate fragments [9]. Actually, it reflects the vigorous character of the ablation process rather than the absence of ablation.

The transparency of the top part of the plume indicates that during the initial ablation phase tissue water is completely vaporized and biomolecules are thermally dissociated into volatile fragments. This requires temperatures above 1000 °C. The subsequent ejection of larger, non-transparent tissue fragments is, for liver, driven by a phase explosion of the tissue water because the tissue matrix is weaker than the pressure developed during the phase separation [1, 3]. The ejection comes to an end when the ablation front reaches a depth where the temperature drops below the stability limit of the superheated tissue water. The average density of the transparent part of the ablation plume is probably not less than that in the particle cloud, but the size distribution of the fragments differs considerably.

For the ablation of skin at a radiant exposure of 5.4 J/cm², the photographs presented in Fig. 5 reveal a slightly different picture. During the initial part of the laser pulse, the extracellular matrix is able to withstand the pressure rise arising from the phase explosion and the subsequent confined boiling process. After 36 ns, the tissue surface is elevated but still intact. Afterwards the ongoing temperature and pressure rise results in the generation of transparent ablation products, probably by thermal dissociation of the biomolecules together with the vaporization of the tissue water. After 120 ns particulate tissue fragments become visible. Their ejection indicates that the temperature has dropped below the value required for thermal disintegration of the matrix. The ejection of tissue fragments ceases when the ablation front reaches a depth where the vapour pressure drops below the tensile strength of the extracellular tissue matrix. The actual strength of the matrix will probably differ considerably from literature values determined under quasi-static loading. It is influenced both by the large strain rates reached during laser ablation and by temperature, whereby both parameters have opposite effects [1, 10]. While large strain rates increase the ultimate tensile strength of the tissue matrix, it is weakened by thermal denaturation.

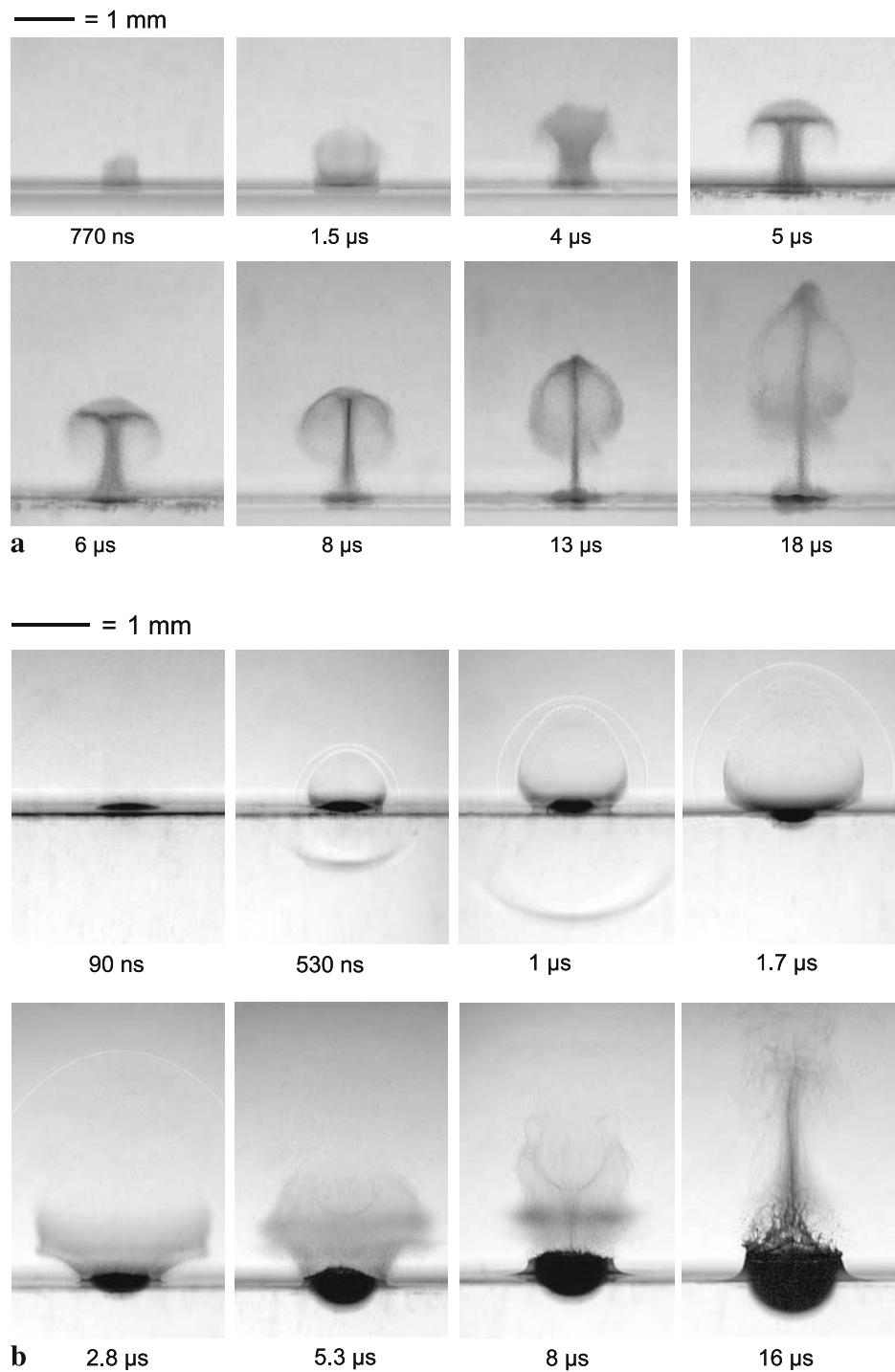


FIGURE 1 Water ablation by a Q-switched Er:YAG laser pulse at radiant exposures of (a) 0.12 J/cm² and (b) 1.4 J/cm². The irradiated spot size was 1 mm in both cases. Ablation is characterized by a succession of explosive vaporization, shock-wave emission, and droplet ejection. In (a), almost the entire plume is filled with droplets resulting from a phase explosion of the superficial water volume. After 5 μs, the plume interaction with the ambient air results in ring vortex formation. In (b), the upper part of the plume is transparent, indicating complete vaporization of the uppermost liquid layer. After 1.5 μs, an “inner shock wave” propagating toward the water surface is visible within the ablation plume. After about 5 μs, this shock wave begins to deform the droplet cloud, and it disturbs the ring vortex formation. The recoil of the ablation products results in a shock wave in the liquid water, an indentation of the water surface, and the expulsion of a large mass of liquid water

3.2 Origin of large volumetric energy densities

It is not self-evident why temperatures more than one order of magnitude above the boiling point of water and large volumetric energy densities corresponding to a super-

critical state of the matter should be reached in pulsed tissue ablation, considering that ablation becomes a volumetric process as soon as the spinodal limit is exceeded and a phase explosion sets in [1]. An important factor contributing to the high volumetric energy densities achieved in nanosecond

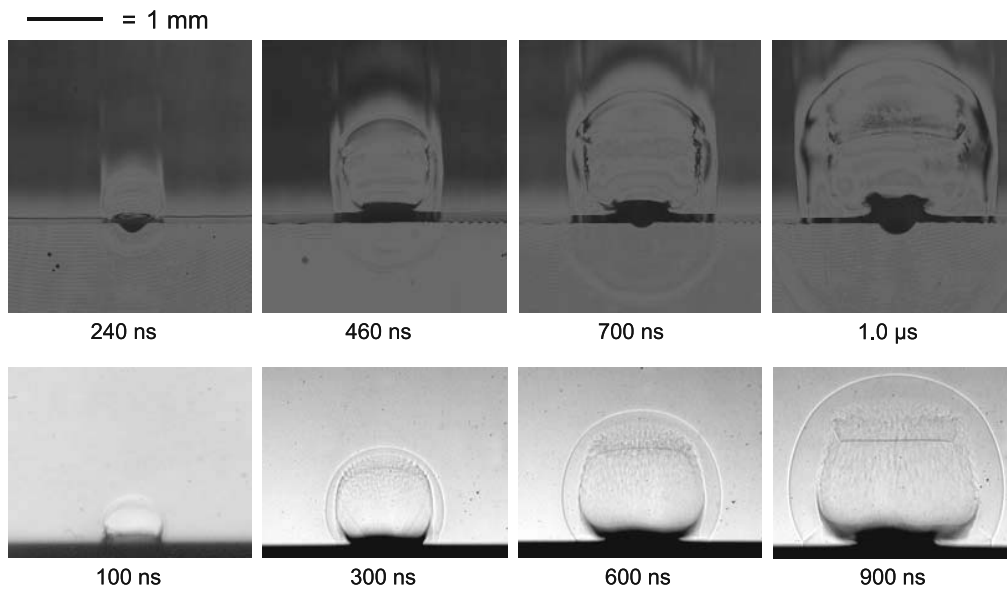


FIGURE 2 Early phase of Q-switched Er:YAG laser ablation of water at 5.4-J/cm^2 radiant exposure and 0.5-mm spot size. *Upper row*: dark-field Schlieren photographs. *Lower row*: bright-field photographs. The inner shock wave is much stronger than with 1.4J/cm^2 (Fig. 1). A later ablation phase is depicted in Fig. 7

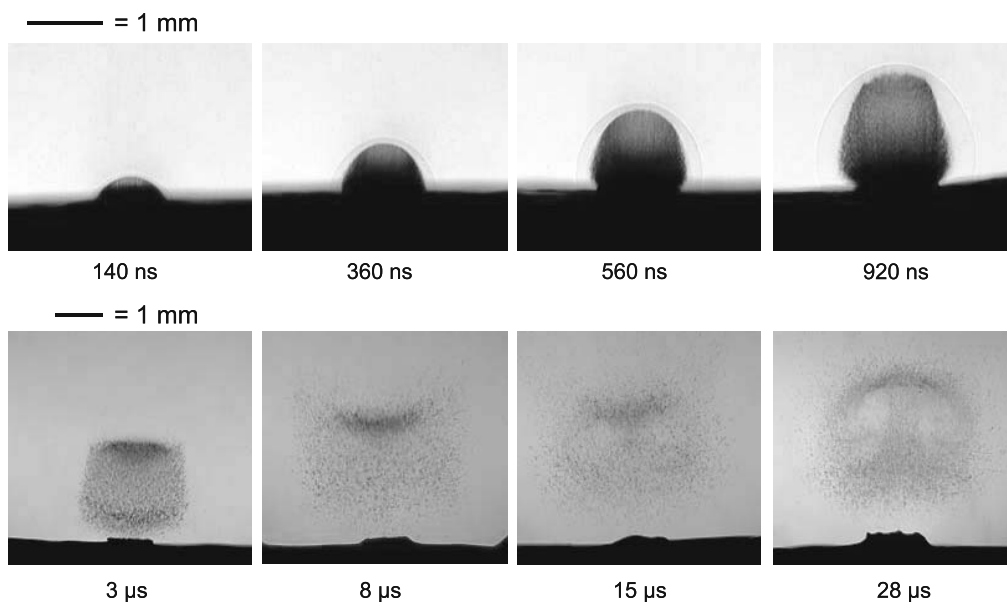


FIGURE 3 Liver ablation at a radiant exposure of 1.4J/cm^2 and 1-mm spot size. The ablation plume consists of fine liver fragments and drives a shock wave that detaches from the plume after about $1\ \mu$ s. The recoil results in a deformation of the surface of the liver sample. During the time interval 1– $10\ \mu$ s after the laser pulse, the particle cloud in the ablation plume is decelerated and deformed by an ‘inner shock wave’ propagating toward the sample surface. Afterwards, a ring vortex is formed by the ongoing particle and vapour flow arising from the sample surface

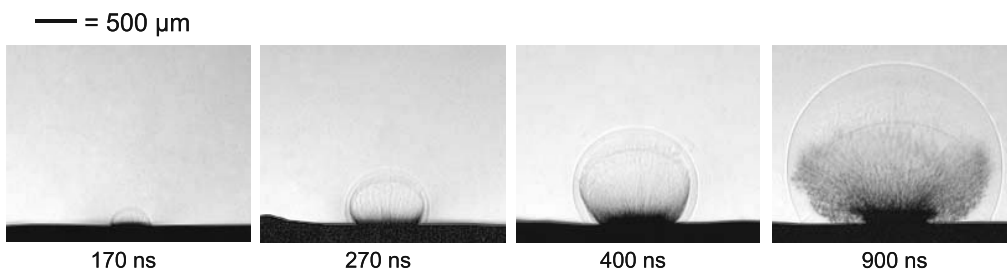


FIGURE 4 Early phase of liver ablation at 5.4-J/cm^2 radiant exposure and 0.5-mm spot size. During a 200-ns-long time interval after the beginning of the laser pulse, the ablation plume is transparent and probably consists of water vapour and volatile fragments of thermally dissociated biomolecules. Afterwards, liver particles are ejected. The frames taken after 340 ns and 820 ns show the inner shock wave and the initial phase of the recoil-induced material expulsion. The late phase is depicted in Fig. 8

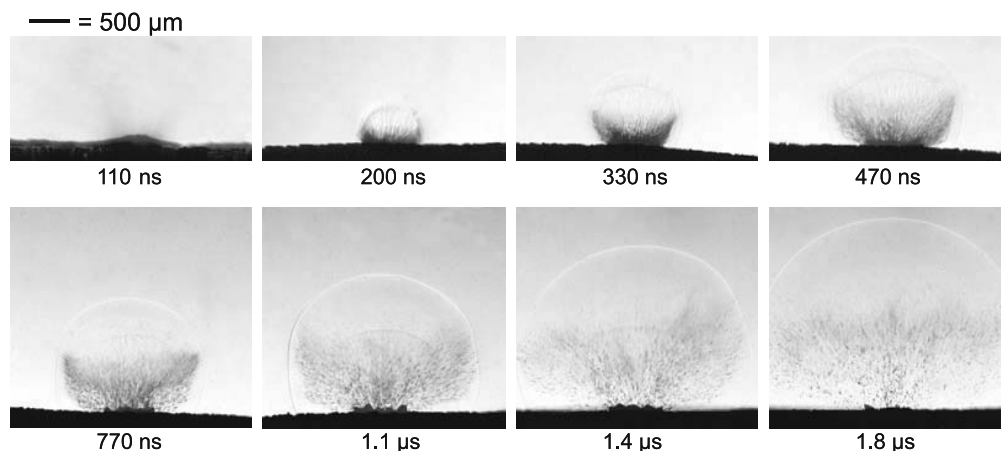


FIGURE 5 Ablation of skin at 5.4-J/cm^2 radiant exposure and 0.5-mm spot size. The plume consists initially only of gas (water vapour and thermally dissociated biomolecules), as in the case of liver ablation. After 120 ns , particulate skin fragments are ejected. A recoil-induced tissue expulsion does not occur

laser ablation is the recoil stress produced by the ablation of superficial target layers. At the beginning of the laser pulse, ablation is governed by non-equilibrium surface vaporization. The vapour pressure above the surface has not yet reached the saturation vapour pressure corresponding to the surface temperature, and the phase transition at the surface therefore proceeds very fast [11]. During this phase, the recoil stress is still small [11], and thus a phase explosion occurs when the temperature reaches the spinodal limit [1]. With the onset of the phase explosion, ablation becomes a volume process, and the recoil stress rises rapidly. The recoil stress suppresses energy dissipation in deeper tissue layers through volumetric phase transitions such as phase explosion or explosive boiling that would occur at ambient pressure [12]. The ongoing absorption of laser energy can thus drive the thermodynamic state of these layers into the supercritical regime. The ablation of deeper layers is delayed until the volumetric energy density becomes sufficiently high to result in a phase transition that can overcome the recoil stress. Evidence for the influence of recoil stress on the thermodynamic state of the target material during the laser pulse is provided by molecular dynamics simulations indicating that recoil stresses begin to develop during the initial part of the laser pulse [10]. Moreover, Polyvinylidene Fluoride (PVDF) transducer measurements of the stresses produced during Q-switched Er:YSGG laser ablation of skin indicated that the peak amplitude of the recoil stress is reached shortly after the peak of the laser pulse when ablation is performed at $2.5\times$ ablation threshold [13]. As shown in Fig. 9 in Sect. 5 below, it occurs even earlier for larger radiant exposures. The delay of the ablation of deeper tissue layers by the recoil stress may well last beyond the end of the laser pulse and is probably one reason for the long duration of primary material ejection visible in Figs. 1, 3, and 5.

	Shock wave in air (m/s)	Ablation plume (m/s)	Droplets, or tissue fragments (m/s)
Water	4200	4100	280
Liver	3500	3400	800
Skin	2700	2600	1700

TABLE 1 Maximum velocities of the shock wave in air, the ablation plume, and particulate tissue fragments in the early phase of ablation at 5.4-J/cm^2 radiant exposure

3.3 Plume dynamics

Due to the high volumetric energy density in the target material produced in Q-switched Er:YAG laser ablation, the initial expansion velocity of the ablation plume is very large (for 5.4-J/cm^2 radiant exposure up to 12 times larger than the sound velocity in air), and drives the emission of an equally fast shock wave. The initial propagation velocities of the shock wave, of the ablation plume, and of particulate tissue fragments are summarized in Table 1. The observed shock-wave and plume velocities correlate with the water content of the different investigated materials that is largest for pure water and smallest for the stratum corneum at the skin surface. A lower water content is associated with a smaller volumetric energy density in the target material and thus with a less vigorous ablation process. By contrast, the velocity of particulate tissue fragments in skin ablation is larger than the velocity of droplets ejected in water ablation. This is because the temperature required for thermal dissociation of the tissue matrix into volatile products is considerably higher than the temperature required for complete vaporization of water. Therefore, tissue fragments become visible very early in the ablation process (after less than 120 ns) when the temperature drops below the level required for thermolysis. At this time, the pressure driving the ejection is still very high. By contrast, droplet ejection from water starts only after about 300 ns when the pressure produced by the phase transition has decayed to a lower level resulting in smaller values of the ejection velocity.

The propagation of the ablation plume exhibits a very complex dynamics. The plume expansion is initially nearly spherical, but after $1\text{--}2\ \mu\text{s}$ the propagation in the forward direction starts to dominate. For small radiant exposures, the interaction of the piston-like forward movement with the ambient air at rest results in ring vortex formation (Fig. 1a). For larger radiant exposures, a region of high density and pressure is created at the contact front between plume and surrounding air. The molecules and molecular clusters propagating with the plume possess a non-zero average velocity. When they collide with air molecules that are, on average, at rest, they are partially reflected back into the plume. This reflection leads to the formation of an internal shock wave that begins to propagate toward the target surface when the rarefaction from the

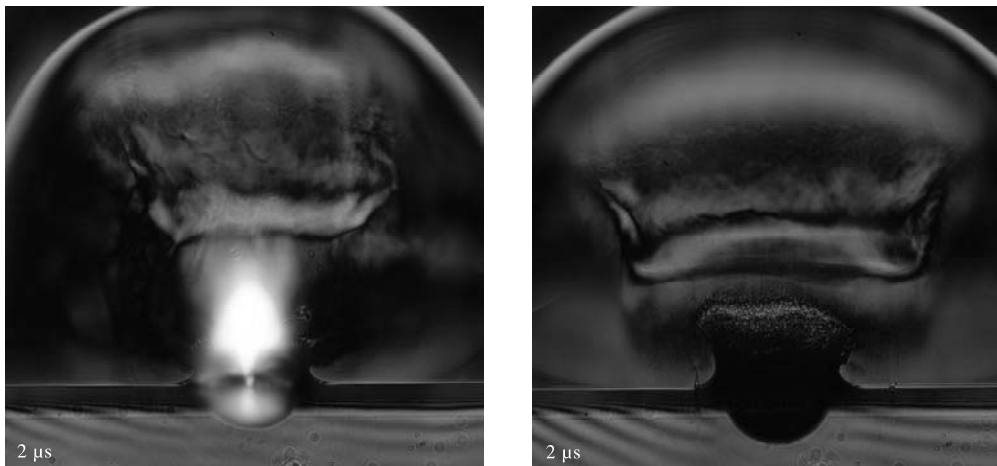


FIGURE 6 Dark-field images of water ablation at $5.4\text{-J}/\text{cm}^2$ radiant exposure with and without plasma formation. The plasma originates in hot spots at the water surface and grows into the incoming laser beam. The recoil-induced cavity is considerably smaller in the case with plasma formation due to the ‘shielding’ of the target by light absorption in the plasma

plume expansion has reduced the pressure in the plume considerably below its initial value [14, 15]. The internal shock wave is faintly visible in Fig. 1b, and appears with even better contrast in Figs. 2, 4, and 5. It begins to interact with the particles and droplets in the plume about $1\ \mu\text{s}$ after the laser pulse, and deforms the shape of the particle cloud during a time interval lasting about $10\ \mu\text{s}$, as visible in Figs. 1 and 3. In this way, the ring vortex formation is suppressed for a while, but finally it emerges from the ongoing particle and vapour flow rising from the sample surface (last frame of Fig. 3).

3.4 Plasma formation

At a radiant exposure of $5.4\text{ J}/\text{cm}^2$, blue plasma radiation was occasionally observed in water ablation, and slightly more frequently in liver and skin ablation. The plasma originated from ‘hot spots’ of the laser beam at the target surface and extended $1\text{--}2\ \text{mm}$ into the surrounding air (Fig. 6). With plasma formation, the kinetics of phase transitions becomes even more complex than described above. Due to its elongated shape, the plasma markedly modifies the laser-induced shock-wave generation. The absorption of optical energy within the plasma diminishes the energy deposition in the target (‘plasma-induced shielding’) and thus reduces the recoil-induced deformation of the target surface. The latter becomes obvious by comparison between the depths of the cavities formed with and without plasma formation. Cummings and Walsh reported the detection of a luminous plume in Q-switched Er:YAG laser ablation of liver and skin by means of a photodiode [16]. However, they did not attribute this to plasma radiation but to an exogenous chemical reaction in the plume. On our photographs, we did not find any evidence for a flame originating from a burning process.

4 Recoil-induced material expulsion

For liquids and mechanically weak tissues, the recoil induced by the primary ablation processes results in an indentation of the target surface and a powerful expulsion of material at the periphery of the irradiated spot that is presented in Figs. 7 and 8 for the ablation of water and liver at a radiant exposure of $5.4\text{ J}/\text{cm}^2$. This phase of secondary material expulsion lasts about $500\ \mu\text{s}$ for liver ablation, and for water ablation it is not entirely completed until almost one second

after the laser pulse. Thus, the total duration of the ablation process is 10 000 to 10 million times longer than the laser pulse releasing it. For skin, no recoil-induced expulsion is observed due to the large mechanical strength of this tissue (see Fig. 5). Therefore, ablation ceases after about $7\ \mu\text{s}$.

Cummings and Walsh used a pump–probe setup for the investigation of the dynamics of liver and skin ablation using Q-switched Er:YAG laser pulses. They observed ‘spikes of probe blockage occurring many microseconds after laser radiation has ceased’ and attributed this to ‘bolus-type removals of tissue as in a series of microexplosions’ [16]. The present investigations demonstrate that only during the first few microseconds after the laser pulse when heat is still retained in the tissue are microexplosions inside the target the driving force for ejection. Post-pulse ablation at later times is due to recoil-induced material expulsion.

Zweig, Frenz and coworkers were the first to consider material expulsion by pressures originating from the ablation plume to be a contributing factor to pulsed tissue ablation [17–19]. However, they did not focus attention on the recoil pressure but assumed that the expulsion of a liquefied tissue layer is driven by radial pressure gradients in the ablation plume that are directed parallel to the target surface. These gradients were assumed to originate from the radial variations of irradiance within a Gaussian beam that would result in radial variations of the vapour pressure in the plume when ablation is driven by surface vaporization. Zweig correctly predicted that these effects are relevant only for ablation using microsecond pulses and very small spot sizes, and that they ‘... become insignificant if the liquid cannot transverse the irradiated spot during the laser pulse, as is typically the case for Q-switched pulses’ [19]. However, he did not proceed to analyse the effects of the recoil pressure. These effects are very pronounced for nanosecond laser pulses where they are capable of producing large material-removal rates and fast ablation plumes.

A key to a better understanding of recoil-induced material expulsion is provided by the observation that it resembles the dynamics produced by the impact of liquid droplets in bulk liquid that has already been investigated in considerable detail [20, 21]. The recoil produces an indentation of the target surface that grows into a hemispherical bubble as shown in Fig. 1b for water ablation at $1.4\text{ J}/\text{cm}^2$. Because

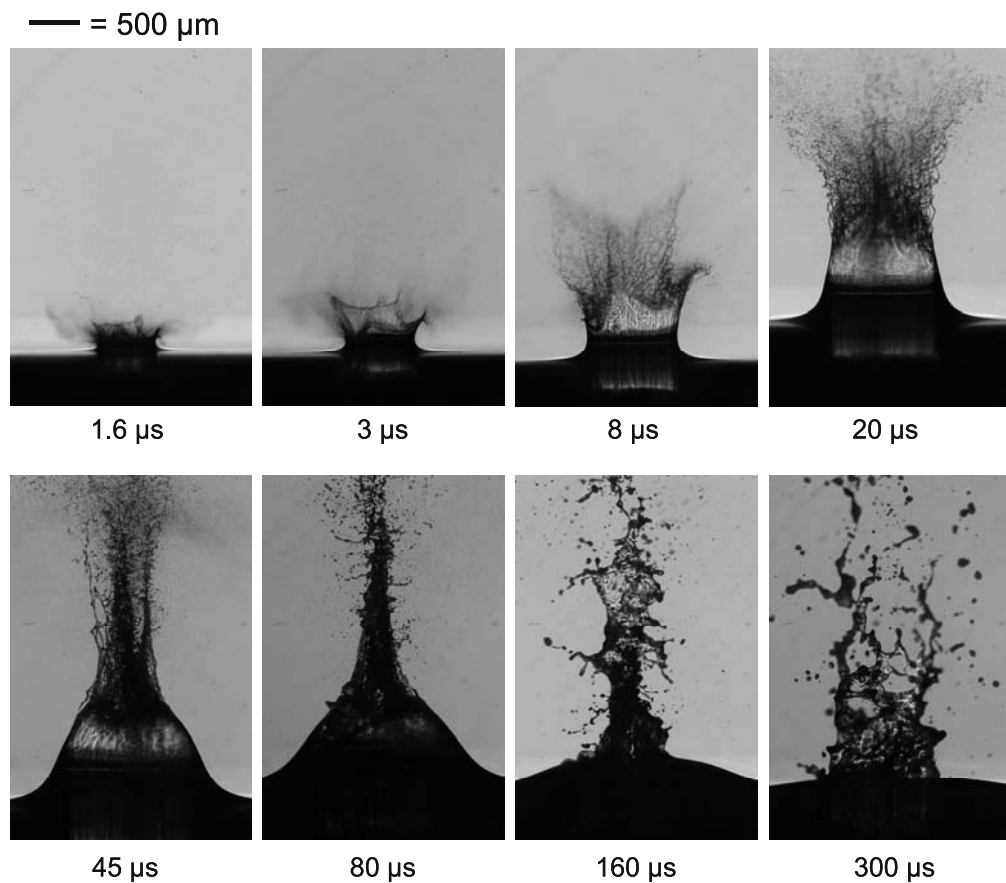


FIGURE 7 Late phase of water ablation at $5.4\text{-J}/\text{cm}^2$ radiant exposure and 0.5-mm spot size. During the first $20\ \mu\text{s}$, the plume dynamics is characterized by a powerful recoil-induced expulsion of liquid water at the periphery of the irradiated spot producing a cylindrical liquid film that at its upper rim decays into droplets. After about $50\ \mu\text{s}$, underpressure inside the recoilgenerated cavity, and surface tension have led to a contraction of the cylindrical liquid film into a conical shape, whereby the fluid contained in the liquid film merges into a jet-like flow. The jet disintegrates soon afterwards due to hydrodynamic instabilities but the dynamics above and below the water surface continues for about $0.5\ \text{s}$ (not shown here)

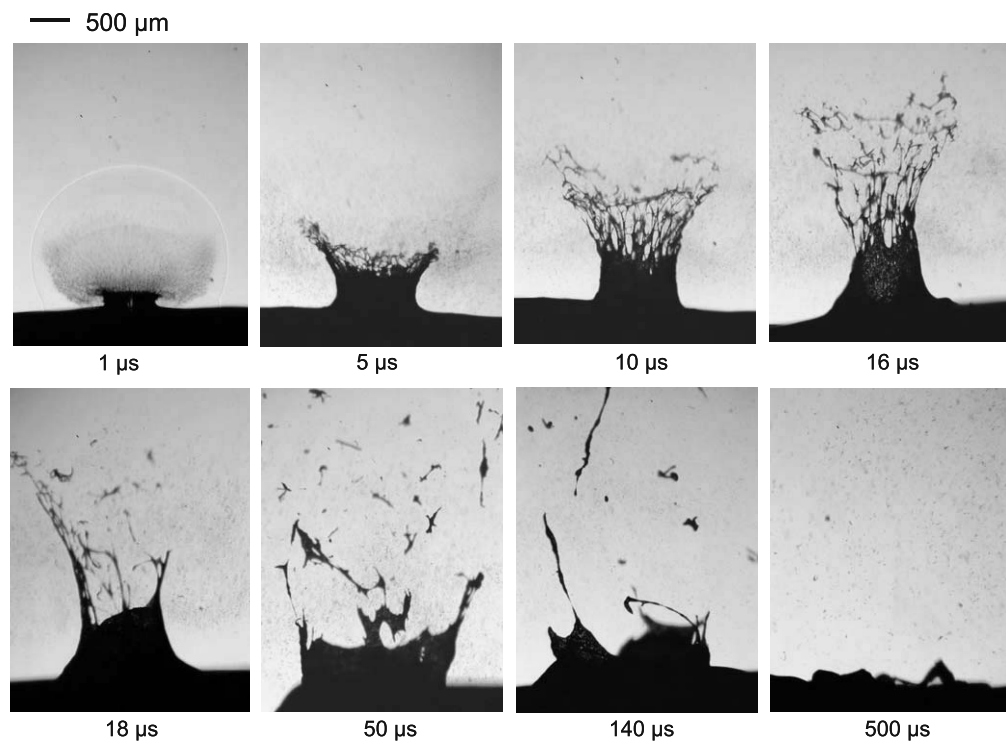


FIGURE 8 Late phase of liver ablation at $5.4\text{-J}/\text{cm}^2$ radiant exposure and 0.5-mm spot size. Similar to the case of water ablation, recoil of primary ablation products results in a powerful expulsion of a tissue 'film' at the periphery of the ablation spot that then decays into large tissue fragments

of the incompressibility of the target material, the displaced fluid must flow in the radial direction toward the periphery of the impacted area where it collides with the surrounding material and is extruded as a cylindrical film that then dis-

solves into a fine spray. At $5.4\text{-J}/\text{cm}^2$ radiant exposure, the initial velocity of the bubble wall is $590\ \text{m}/\text{s}$ (determined from photographs taken at different time delays), and the cylindrical film rises with an average velocity of $150\ \text{m}/\text{s}$ during

the first 20 μs after the laser pulse (Fig. 7). The velocity of the droplets in the splash amounts to 230 m/s. This dynamics is 20 times faster than the sequence of events produced by the impact of water droplets after falling 20 m in a partially evacuated tube that were investigated by Engel [20]. The droplets impacted at a velocity of 19 m/s and produced a film rising with an initial velocity of ≈ 7 m/s. It is not quite clear yet under which conditions soft tissue responds to recoil stress like a liquid, and when it behaves like a solid where spatial variations of the stress tensor rather than the scalar pressure distribution have to be considered to understand material expulsion. However, it is known that the path-lines of plastic deformations in an impacted solid [22] resemble the flow pattern induced by droplet impact on a liquid surface [20].

After about 50 μs the cylindrical film assumes a conical shape in its lower part, and the flow in this film merges into an upwardly directed jet flow. The contraction of the cylindrical flow into a jet flow is partly caused by surface tension, and partly by the under-pressure in the expanding cavity [23]. Later, the jet disintegrates due to hydrodynamic instabilities. The dynamics below and above the water surface continues for almost one second. A similar dynamics and ejection velocities of comparable magnitude have been observed also for the ablation of liver (Fig. 8). However, here the cylindrical tissue film decays into pieces due to inhomogeneities within the tissue before it can contract to form a jet. One can deduce from the similarity of the ejection dynamics in liver and water ablation that a transient hemispherical cavity forms below the target surface also in liver ablation, even though this is not visible in the photographs.

The recoil-induced material expulsion becomes ever more important with decreasing laser-pulse duration. For water ablation, the ejection velocity is 25 m/s when free-running Er:YAG laser pulses of 200- μs duration and 50-J/cm² radiant exposure are used [3], but it amounts to 150 m/s when Q-switched pulses of 70-ns duration and radiant exposure of 5.4-J/cm² are employed. Recoil-induced material expulsion in liver ablation is weak for free-running laser pulses of 50 J/cm² [3], but very vigorous for Q-switched pulses of 5.4 J/cm. Reducing the laser-pulse duration can, therefore, considerably increase the ablation efficiency in soft-tissue ablation. This strategy can be applied in all cases where the speed of ablation is more important than high precision and lack of collateral mechanical damage. For mechanically stronger tissue such as skin, material removal cannot be enhanced by recoil-induced tissue expulsion, but the ablation is more precise in a larger range of radiant exposures than for very soft tissues.

5 Shock waves in air and within the target material

5.1 Shock-wave velocities and pressures

For the ablation of all investigated target materials we used photographs visualizing the shock-wave propagation to determine the shock-wave velocity in air (see Table 1) and to calculate the shock-wave pressure. For water ablation, this method could also be applied to determine the shock-wave parameters within the target material. Figure 9 presents the distances s travelled by the shock waves produced during wa-

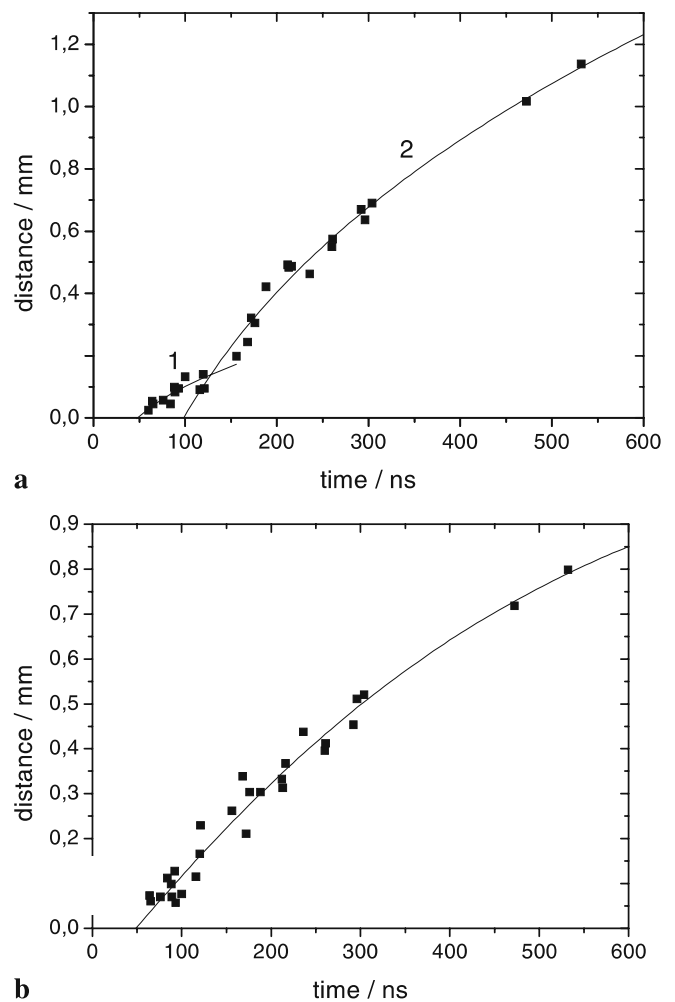


FIGURE 9 Shock-wave propagation in air (a) and water (b) for water ablation at 5.4-J/cm² radiant exposure and 0.5-mm spot size. Curves are fitted by a least mean square fit, and from the slope of these curves the initial shock-wave velocities are determined

ter ablation at 5.4-J/cm² radiant exposure as a function of time t . The initial shock-wave velocities u_s were obtained from curves fitted through the $s(t)$ data for air (Fig. 9a) and water (Fig. 9b). We then used the following relations to calculate the shock-wave pressure p_s in air [24]:

$$p_s = \left[\frac{7}{6} \left(\frac{u_s}{c_0} \right)^2 - \frac{1}{6} \right] p_\infty \quad (1)$$

and in water [25]

$$p_s = c_1 \varrho_0 u_s (10^{(u_s - c_0)/c_2} - 1) + p_\infty. \quad (2)$$

Here ϱ_0 denotes the density of the medium before compression by the shock wave, c_0 is the normal sound velocity in the medium (343 m/s in air, 1483 m/s in water at 20 °C), $c_1 = 5190$ m/s, $c_2 = 25\,306$ m/s, and p_∞ is the atmospheric pressure. Equation (2) is based on the conservation of momentum at the shock front [26]:

$$p_s - p_\infty = u_s u_p \varrho_0 \quad (3)$$

and on the Hugoniot curve data determined by Rice and Walsh [27]:

$$u_p = c_1(10^{(u_s - c_0)/c_2} - 1). \quad (4)$$

A pressure determination from optical observations of the shock-wave propagation is possible only in a parameter range where the shock-wave velocity differs notably from the normal sound velocity in the medium. However, in this regime it is very reliable because the Hugoniot curve data for water and air are well known and no transducer calibration is required.

The data in Fig. 9a indicate that 40–50 ns after the start of the laser pulse a shock wave begins to propagate into the surrounding air at a velocity of about 1500 m/s (fitted curve 1). Later the shock wave is accelerated, seemingly due to an explosive event that takes place about 100 ns after the start of the pulse (i.e. after the peak intensity in the pulse of 70 ns FWHM is reached). The initial speed of the compressive wave produced by this event is 4200 m/s (fitted curve 2). Figure 9b shows that the recoil-induced transient in water starts to propagate about 50 ns after the beginning of the laser pulse with an initial velocity of 2300 m/s. Fit 1 in Fig. 9a represents the plume expansion during the initial ablation phase that involves more superficial target layers. The recoil pressure produced during this phase supports the build-up of a high volumetric energy density in deeper target layers. The faster portion of the shock wave (fit 2) probably originates from the explosive vaporization of a larger, supercritical liquid volume that takes place in the second half of the pulse after a partial release of the recoil pressure. The start of the recoil-induced transient in water approximately coincides with the start of shock wave 1 in air but precedes shock wave 2. One would expect that the vapour explosion producing shock wave 2 would accelerate the recoil-induced transient in water. However, such an influence is not evident from the present data exhibiting a fairly large scatter.

For water ablation at 5.4-J/cm² radiant exposure, the data of Fig. 9 yield an initial shock-wave pressure of 17.5 MPa above the water surface, and of 930 MPa within the water sample. For liver and skin, pressure amplitudes could only be determined above the sample because the shock-wave propagation could not be followed within the opaque tissue. We obtained peak pressure values of 12.1 MPa for liver and 7.2 MPa for skin. These values are lower than for water because the same radiant exposure produces lower volumetric energy densities in materials with lower water content. Assuming that the recoil stress scales with the water content of the target material in the same way as the shock-wave pressure in air, we deduce that the recoil stress in liver and skin amount to about 770 MPa and 590 MPa, respectively, for 5.4-J/cm² radiant exposure. Our results for the recoil stress are consistent with results of measurements with PVDF transducers reported by other researchers. Venugopalan and coworkers [13] obtained recoil stress values of 60 MPa for Q-switched Er:YSGG laser irradiation of skin at 2.5 J/cm², and Könz and coworkers [28] reported values of up to 1000 MPa for Q-switched Er:YAG laser irradiation of the cornea with radiant exposures of up to 15.9 J/cm².

For water ablation, the peak pressure of the shock wave within the water sample is 66 times larger than the shock-wave

pressure in air. This difference indicates that the duration of the pressure transient in air must be much longer than the duration of the recoil transient because, due to conservation of momentum requirements, the impulse per unit area $I = \int p dt$ must be the same in both cases. The duration of the recoil-induced stress transient in Q-switched Er:YAG laser ablation of the cornea was found to be ≈ 120 ns by PVDF transducer measurements [28], and measurements for Q-switched Er:YSGG laser ablation of skin yielded similar results [13]. Considering conservation of momentum, we deduce that the pressure pulse in air should have a duration of several microseconds. This conclusion is supported by the observation that the shock wave detaches from the ablation plume only after about 1 μ s (Figs. 1 and 3). Thus, the pressure driving the plume expansion must be fairly high for a time period of at least 1 μ s, and this is reflected in the duration of the emitted pressure transient.

5.2 Interaction of recoil-induced shock wave and target

The large values of the recoil stress measured during the second half of the laser pulse confirm the assumption of Sect. 3.2 that the phase transitions in the target material during the initial phases of tissue ablation occur under extreme thermodynamic conditions. The recoil stress supports the build-up of high temperatures by the incident laser irradiation enabling thermal dissociation of the extracellular matrix that becomes manifest by the transparency of the top part of the ablation plume in Figs. 4 and 5. Further evidence for the high volumetric energy densities produced during Q-switched Er:YAG laser ablation is provided by the fact that the shock-wave pressure in air produced during ablation of water at 5.4-J/cm² radiant exposure is 40 times larger than the pressure generated during the phase explosion produced by the first spike of a free-running Er:YAG laser pulse of 50 J/cm² [3].

The initial particle velocity u_p behind the recoil-induced shock front in water is expected to be equal to the velocity u_B of the wall of the hemispherical cavity that is produced by the recoil forces [25]. From $u_s = 2300$ m/s and Eq. (4) we obtain $u_p = 400$ m/s. A direct determination of the initial bubble-wall velocity by evaluation of the photographs yields $u_B \approx 590$ m/s, which is larger than the value of u_p determined from the shock-wave propagation. This discrepancy may be due to the fact that after shock-wave detachment the bubble wall continues to be accelerated for a short period of time by the high pressure in the ablation plume.

The peak recoil stress produced during liver ablation at 5.4-J/cm² radiant exposure is 30 000 times larger than the ultimate tensile strength of liver that was determined to be 24 kPa by quasi-static measurements at small strain rates [29]. At first sight, this seems to be a sufficient explanation for the massive recoil-induced tissue ejection and the similarity of the flow of the ejected material with the hydrodynamic flow pattern observed in water ablation (see Figs. 7 and 8). However, no recoil-induced ejection is observed in skin ablation, even though the recoil stress is about 50 times larger than the quasi-static ultimate tensile strength of skin that amounts to about 10 MPa [29, 30]. To explain this discrepancy, it must first be considered that the recoil-induced tensile and shear stresses leading to tissue fracture may be considerably smaller than

the measured compressive recoil stress. Moreover, it is a necessary but not a sufficient condition for recoil-induced tissue expulsion that the recoil stress exceeds the ultimate tensile strength (UTS) of the tissue. Tissue fracture will only occur at sufficiently large strain [1, 29] that may not be achieved by stress transients of very short duration. Material expulsion requires, furthermore, that the material be displaced over a distance comparable to the radius of the ablation spot. The material displacement upon passage of a shock wave with $u_p = 400$ m/s and 120-ns duration, however, amounts to only 48 μm . Material transport over larger distances is due to the expansion of the recoil-produced indentation of the target surface. The driving force for the cavity expansion does not stop when the shock wave detaches but lasts for the period of time during which a high pressure exists in the ablation plume [25, 31], i.e. for a few microseconds. Thus, we have to check whether the pressure in the plume exceeds the mechanical strength of the tissue target. The peak pressure value in the plume is given by the pressure at the shock front in air, which amounts to 11.7 MPa and 9.0 MPa for liver and skin ablation, respectively. The pressure in the plume is considerably larger than the UTS of liver but comparable to the quasi-static UTS of skin. Considering that the pressure in the plume soon drops below its peak value and that the dynamic tensile strength of tissue is higher for the extreme strain rates produced in pulsed laser ablation than the quasi-static values found in the literature [1], it becomes comprehensible that no recoil-induced expulsion was observed in skin ablation.

6 Conclusions

Laser tissue ablation using nanosecond pulses is often considered to be a ‘blow-off’ process that commences after the end of the laser pulse, when the entire optical energy has been deposited into the target, and in which ablation occurs everywhere simultaneously and in the same way. However, our investigation showed that the ablation dynamics starts during the laser irradiation and is characterized by a succession of different phases that produce different types of gaseous and condensed ablation products.

For water and liver ablation, the cascade of primary material ejection processes is followed by a powerful recoil-induced material expulsion and by a dramatic mechanical deformation of the non-ablated material. Such effects are absent for skin. However, shock-wave-induced damage in deeper tissue layers has also been observed for ablation of skin and cornea using laser pulses of nanosecond duration [28, 32]. The influence of recoil-induced expulsion explains why in a previous study using a short-pulse TEA (transverse excitation at atmospheric pressure) CO_2 laser irradiation liver ablation was found to be up to five times more efficient than skin ablation [33]. Both the efficiency of recoil-induced material expulsion and the mechanical collateral effects increase strongly when the pulse duration decreases at equal radiant exposure. Thus, the precision of pulsed laser tissue ablation does not only depend on the optical penetration depth and the pulse duration, but also on the mechanical tissue properties and the radiant-exposure-dependent recoil effects.

With increasing volumetric energy density within the tissue, the ablation dynamics undergoes stepwise changes at

thresholds demarcating either the transition to new types of phase transitions or the incorporation of recoil-induced effects into material removal. As a logical consequence, the time course of ablation must consist of different phases reflecting the spatio-temporal evolution of the volumetric energy density in the target, and the dependence between ablation depth and radiant exposure over a larger range of radiant exposures must be non-linear. Any simple relation between radiant exposure and ablation depth as predicted by heuristic blow-off or steady-state models [1] can only be an approximation for a limited range of radiant exposures.

To date, neither the succession of different types of explosive phase transitions in the primary ablation process nor recoil-induced ejection have been considered in models of laser tissue ablation. However, their theoretical modelling is a prerequisite for a reliable prediction of ablation depth and collateral damage and thus poses an important challenge for future work.

REFERENCES

- 1 A. Vogel, V. Venugopalan, *Chem. Rev.* **103**, 577 (2003)
- 2 A. Vogel, V. Venugopalan, *Proc. SPIE* **4961**, 66 (2003)
- 3 A. Vogel, B. Kersten, I. Apitz, *Proc. SPIE* **4961**, 40 (2003)
- 4 K. Nahen, A. Vogel, *Lasers Surg. Med.* **25**, 69 (1999)
- 5 K. Nahen, A. Vogel, *J. Biomed. Opt.* **7**, 165 (2002)
- 6 E. Hecht, A. Zajac, *Optics* (Addison-Wesley, Reading, MA, 1977)
- 7 V.P. Skripov, E.N. Sinityn, P.A. Pavlov, G.V. Ermakov, G.N. Muratov, N.V. Bulanov, V.G. Baidakov, *Thermophysical Properties of Liquids in the Metastable (Superheated) State* (Gordon and Breach Science, New York, 1988)
- 8 L.V. Zhigilei, *Appl. Phys. A* **76**, 339 (2003)
- 9 J.T. Walsh, T.F. Deutsch, *Appl. Phys. B* **52**, 217 (1991)
- 10 L.V. Zhigilei, E. Leveugle, B.J. Garrison, Y. Yingling, M.I. Zeifman, *Chem. Rev.* **103**, 321 (2003)
- 11 A.D. Yablon, N.S. Nishioka, B.B. Mikić, V. Venugopalan: *Proc. SPIE* **3343**, 69 (1998)
- 12 Q. Lu, *Phys. Rev. E* **67**, 016 410 (2003)
- 13 V. Venugopalan, N.S. Nishioka, B.B. Mikić, *Biophys. J.* **70**, 2981 (1996)
- 14 N. Arnold, J. Gruber, J. Heitz, *Appl. Phys. A* **69**, S87 (1999)
- 15 H.L. Brode, *Phys. Fluids* **2**, 217 (1959)
- 16 J.P. Cummings, J.T. Walsh, *Proc. SPIE* **1646**, 242 (1992)
- 17 A.D. Zweig, H.P. Weber, *IEEE J. Quantum Electron.* **QE-23**, 1787 (1987)
- 18 M. Frenz, V. Romano, A.D. Zweig, H.P. Weber, N.I. Chapliev, A.V. Silenok, *J. Appl. Phys.* **66**, 4496 (1989)
- 19 A.D. Zweig, *J. Appl. Phys.* **70**, 1684 (1991)
- 20 O.G. Engel, *J. Appl. Phys.* **37**, 1798 (1966)
- 21 A. Prosperetti, H.N. Oguz, *Annu. Rev. Fluid Mech.* **25**, 577 (1993)
- 22 F.P. Bowden, J.H. Brunton, *Proc. R. Soc. Lond. A* **263**, 433 (1961)
- 23 C.L. Mader, M.L. Gittings, *Sci. Tsunami Hazards* **21**, 91 (2003)
- 24 L.D. Landau, E.M. Lifschitz, *Hydrodynamik* (Akademie, Berlin, 1991), §89
- 25 A. Vogel, S. Busch, U. Parlitz, *J. Acoust. Soc. Am.* **100**, 148 (1996)
- 26 G.E. Duvall, G.R. Fowles, *Shock Waves. In High Pressure Physics and Chemistry*, ed. by R.S. Bradley (Academic, New York, 1963), pp. 209–291
- 27 M.H. Rice, J.M. Walsh, *J. Chem. Phys.* **26**, 824 (1957)
- 28 F. Könz, M. Frenz, H. Pratisto, H.P. Weber, H. Lubatschowski, O. Kernani, W. Ertmer, H.J. Altermatt, T. Schaffner, *Proc. SPIE* **2077**, 78 (1994)
- 29 F.A. Duck, *Physical Properties of Tissue* (Academic, London, 1990)
- 30 F.H. Silver, *Biological Materials: Structure, Mechanical Properties, and Modeling of Soft Tissue* (New York University Press, New York and London, 1987)
- 31 R. Fabbro, J. Fournier, P. Ballard, D. Devaux, J. Virmont, *J. Appl. Phys.* **68**, 775 (1990)
- 32 S. Watanabe, T.J. Flotte, D.J. McAuliffe, S.L. Jacques, *J. Invest. Dermatol.* **90**, 761 (1988)
- 33 J.T. Walsh, T.F. Deutsch, *IEEE Trans. Biomed. Eng.* **36**, 1195 (1989)